Comparison of fluorine-18 and bromine-76 imaging in positron emission tomography

Maria João Ribeiro[1,2], Pedro Almeida[1], Daniel Strul[1], Nuno Ferreira[1,2], Christian Loc'h[1], Vincent Brulon[1], Régine Trébossen[1], Bernard Mazière[1], Bernard Bendriem[1]

[1] Service Hospitalier Frédéric Joliot, CEA, Orsay, France
[2] Serviço de Biofísica – IBILI – FMC, Coimbra, Portugal

Received 30 January and in revised form 18 March 1999

Abstract. State of the art positron emission tomography (PET) systems allow for scatter and attenuation correction. However, the size of the structure being studied and the region of interest (ROI) chosen also influence the accuracy of measurements of radioactive concentration. Furthermore, the limited spatial resolution of PET tomographs, which depends, among other factors, on the range of positrons in matter, can also contribute to a loss in quantitation accuracy. In this paper we address the influence of positron range, structure size and ROI size on the quantitation of radioactive concentration using PET. ECAT EXACT HR+ (HR+) and ECAT 953B/31 (ECAT 953B) PET systems were used in phantom acquisitions performed with two radioisotopes with different positron ranges. The 3D Hoffman phantom was scanned on both scanners with both radioisotopes, to visually analyse the image quality. A resolution phantom having six spheres of different diameters in a Plexiglas cylinder was used to calculate the values of the contrast recovery coefficient or hot spot recovery coefficient and of the spill-over or cold spot recovery coefficient under different imaging conditions used in clinical routine at our institution. Activity ratios were varied between 2 and 30 or between 0.4 and 200 by filling the spheres with fluorine-18 or bromine-76 respectively and the cylinder with ^{11}C. Dynamic scans were performed on each scanner. Data were reconstructed using the same parameters as are used in clinical protocols. The variations in sphere and cylinder activities with time were fitted using the function $M(t)=k_1 \cdot A(t)+k_2 \cdot B(t)$, where $M(t)$ is the radioactivity concentration measured in an ROI placed on each sphere and $A(t)$ and $B(t)$ represent the true radioactivity concentrations present at time t in the spheres and in the cylinder respectively. k_1 and k_2 are factors representing the contrast recovery coefficient and the spill-over from surrounding activity on measurements respectively. The visual analysis of images obtained using a 3D Hoffman phantom showed that image resolution and image contrast between different regions are radioisotope dependent and clearly better when using ^{18}F. Linear profiles taken on these images confirmed the visual assessment. For a given scanner, the k_1 values obtained with ^{18}F were systematically higher than those measured using ^{76}Br in the same machine (especially for the smaller spheres) when using the same ROI. For a sphere of a particular diameter, the use of a wider ROI resulted in lower quantitative accuracy when using the same isotope and the same camera. Lower quantitative accuracy was found for smaller spheres for all ROI sizes used in image analysis. For the same scanner and for a similar imaging situation (same sphere and same ROI), it was found that k_1 and k_2 values depend on the radioisotope used. For the same isotope and tomograph, the k_1 values obtained decreased with the size of the structures imaged, as well as with the increase in ROI size. The use of a tomograph with better spatial resolution (HR+, rather than ECAT 953B) greatly increased the k_1 values for ^{18}F while only a mild improvement in these values was observed for ^{76}Br. The use of ^{76}Br led to k_2 values that were slightly higher than those measured using ^{18}F. These differences may have been due to the difference in the range of the positrons emitted by the radioisotopes used in this study. The measurements performed in this study show that the comparison of studies obtained on the same camera depends on the radioisotope used and may require the adaptation of ROI size between examinations. Marked differences are visible if the positron ranges of such radioisotopes are very different. Therefore, when employing commercially available tomographs and imaging protocols used in clinical routine, the effects of differences in positron range on image quality and quantitation are noticeable and correction for these effects may be of importance. With the arrival of PET imaging systems with better spatial resolution (close to 2 mm full-width at half-maximum for animal PET systems), positron range will have an increasing influence on the image quality and on the choice of radioisotope for a given application.

Correspondence to: M.J. Ribeiro, Service Hospitalier Frédéric Joliot, CEA, 4, place du Général Leclerc, F-91401 Orsay Cedex, France

Key words: Positron emission tomography – Quantitation – Regions of interest – Hot spot recovery coefficient – Cold spot recovery coefficient – Positron range

Eur J Nucl Med (1999) 26:758–766

Introduction

One of the advantages of positron emission tomography (PET) is the use of the positron emitters carbon-11, nitrogen-13 and oxygen-15, which are radioisotopes of the most abundant atoms present in living beings. However, the half-lives ($T_{1/2}$) of these radioisotopes are short and may limit the use of long acquisition protocols. This limitation can be overcome by the use of longer half-life positron emitters like fluorine-18 or bromine-76.

Fluorine-18 ($T_{1/2}$=108.9 min) is currently used for the production of ^{18}F-fluorodesoxyglucose (^{18}F-FDG), which is playing an increasingly important role in oncology [1]. Additionally, 6-^{18}F-L-3,4-fluorodihydroxyphenylalanine or L-dopa (^{18}F-L-dopa), a precursor of dopamine, is currently used for the study of Parkinson's disease [2, 3].

Bromine-76 ($T_{1/2}$=972 min) can be attractive for the study of radioligands equilibrating slowly in vivo. Using ^{76}Br, target areas may be optimally visualised at later times after the decrease in non-specific uptake. Examples of ^{76}Br-labelled molecules are dopamine D_2 receptor radioligands, such as ^{76}Br-bromospiperone (^{76}Br-BSP) [4] and *m*-acetylcholine receptor ligands such as ^{76}Br- bromodexetimide (^{76}Br-BDEX) [5,6]. Moreover, some molecules of interest in nuclear medicine allow alternative labelling routes using either ^{76}Br or iodine-123, for example. Examples are ^{76}Br-lisuride and ^{123}I-iodolisuride [7] or ^{76}Br-FLB457 and its iodinated analogue ^{123}I-epidepride [8].

The radioactive concentration uptake values obtained from molecules targeting neuroreceptor populations can be used to construct mathematical models from which to calculate, for example, the concentration values of dopamine receptors. However, these models lack a practical purpose if accurate quantitation of PET data is not available.

In cerebral PET, a great number of factors affect the accuracy of activity measurements. These factors include the size, the shape and the position of cerebral structures as well as the spatial resolution of the tomograph used. Difficulties in defining the localisation of regions of interest (ROI) and their dimensions with respect to cerebral anatomy can also affect the quantitative outcome. In fact, some authors have indicated that the ROI size may have a significant impact on quantitation using PET. The radioactivity concentration values measured in the caudate nuclei, for example, may decrease by nearly 40% if the diameter of the ROI used in the analysis is increased from 1 cm to 2 cm [9]. As a result, the majority of absolute values reported for various cerebral structures using PET are not precise measurements of the real activity concentration values [10]. However, the size of the area sampled must be large enough for the effect of the image noise on quantitation to be acceptable.

The distance travelled by the positron prior to its annihilation on tissue has also been identified as an additional source of blurring in PET [11, 12]. This distance is relatively small for lower energy positron emitters such as ^{18}F and ^{11}C (maximum kinetic energy of positron <1 MeV), compared with higher energy positron emitters such as ^{15}O, ^{68}Ga and ^{76}Br (maximum kinetic energy of positron >1.7 MeV). To our knowledge, no published works have addressed the effects of positron range on the accuracy of radioactivity concentration measurements using PET under conditions of clinical routine.

Our department currently uses molecules labelled with ^{76}Br or ^{18}F for the study of the dopaminergic system. The use of these radioisotopes may result in different intrinsic spatial resolution losses in PET (the positron range is 5.3 and 0.7 mm for ^{76}Br and ^{18}F, respectively) [13]. This can hinder the comparison of studies of the same anatomical regions using radiotracers labelled with different radioisotopes.

In this paper, we address the influence of positron range, structure size and ROI size on the quantitation of radioactive concentration in clinical routine PET.

Material and methods

Positron emission tomographs. Studies were performed on two PET systems from Siemens/CTI (Knoxville, Tenn., USA): a brain imaging system, the ECAT 953B/31 (ECAT 953B) was used to acquire 2D scans and a whole-body scanner, the ECAT EXACT HR+ (HR+), was used to acquire 3D data.

The ECAT 953B is able to acquire 31 simultaneous slices with a slice thickness of 3.4 mm. Its sensitivity is approximately 4 counts/(Bq/ml) in 2D mode. The in-plane average intrinsic resolution is 6.0 mm full-width at half-maximum (FWHM) and the axial average intrinsic resolution is 5.0 mm FWHM. The ECAT 953B has a field of view (FOV) of 10.8 cm in the axial direction [14–16].

The HR+ can acquire 63 simultaneous slices with a thickness of 2.4 mm. This scanner is characterised by average axial and transaxial intrinsic resolutions at the centre of the FOV of 4.1 mm FWHM and 4.3 mm FWHM respectively. Its axial FOV is 15.5 cm and its sensitivity is approximately 27 counts/(Bq/ml) in 3D mode [17, 18].

Measurements of spatial resolution. The spatial resolutions (FWHM) for ^{76}Br and ^{18}F were measured using linear sources placed inside a cylindrical phantom (20 cm in diameter) filled with water, 5 cm away from the centre of the FOV. Data were reconstructed using the protocols used for the resolution phantom experiences.

Phantoms. A 3-D brain phantom (Hoffman phantom) was used to simulate the study of cerebral blood flow and metabolism [19]. ^{76}Br and ^{18}F were used on each scanner to perform a visual analysis of image resolution and image contrast.

Table 1. Areas (cm^2) of the ROIs used in the analysis of the images obtained using the resolution phantom on both scanners. For each sphere the circle areas (in cm^2) corresponding to the equator of each sphere are indicated

Sphere	ROI_A (cm^2)		ROI_B (cm^2)		ROI_C (cm^2)		ROI_D (cm^2)		ROI_E (cm^2)		ROI_F (cm^2)	
	ECAT	HR+	ECAT	HR+	ECAT	HR+	ECAT	HR+	ECAT	HR+	ECAT	HR+
Sphere 1 (8.9 cm^2)	10.0	10.0	5.0	5.2	2.8	3.0	2.3	2.2	1.1	1.2	0.4	0.5
Sphere 2 (6.0 cm^2)	6.7	6.9	3.2	3.9	2.1	2.4	1.3	1.3	0.8	0.9	0.4	0.5
Sphere 3 (3.9 cm^2)	4.2	4.7	2.5	2.6	1.8	1.9	1.2	1.2	0.7	0.6	0.4	0.5
Sphere 4 (1.9 cm^2)	2.0	2.3	1.6	2.1	1.1	1.3	0.9	1.2	0.6	0.5	0.4	0.4
Sphere 5 (1.4 cm^2)	1.7	1.7	1.3	1.5	0.9	1.2	0.6	0.6	0.5	0.5	0.4	0.4
Sphere 6 (0.8 cm^2)	1.1	1.1	0.7	1.0	0.5	0.6	0.5	0.5	0.4	0.4	0.3	0.3

A resolution phantom (Deluxe ECT Phantom, Data Spectrum Corporation, Hillsborough, N.C., USA) was used to evaluate the dependence of accuracy of activity quantitation on radioisotope positron range, structure size and ROI size. The phantom consists of fillable spheres with inner diameters of 33.6, 27.8, 22.1, 15.5, 13.2 and 10.2 mm (spheres 1–6 respectively), corresponding to equator circle areas of 8.9, 6.0, 3.9, 1.9, 1.4 and 0.8 cm^2, which are placed inside a Plexiglas cylinder (18.6 cm in height and 21.6 cm in diameter). The centre of each sphere is located on the same circle, 5 cm away from the phantom axis.

Imaging protocols. The studies performed using the 3-D brain phantom employed the same radioactivity concentration of ^{76}Br (16 kBq/ml) on both scanners. In the case of ^{18}F, the radioactive concentrations used on HR+ and on ECAT 953B were 68 kBq/ml and 56 kBq/ml respectively. All studies used one static acquisition of 120 min except in the case of the ^{18}F scan acquired on the HR+, which lasted for 20 min. One ^{76}Br and one ^{18}F image were obtained using each scanner.

In the case of the resolution phantom, the spheres were filled with uniform solutions of ^{76}Br or ^{18}F. The cylinder (background) was filled with a uniform solution of ^{11}C. The activity ratios between the spheres and the background varied between 0.4 and 200 in the case of ^{76}Br and between 2 and 30 in the case of ^{18}F. The experiments performed on the ECAT 953B used dynamic scans of 70 frames acquired over a total of 140 min. Studies performed using the HR+ and the same phantom used dynamic sets of 2-min length acquisitions separated by 2-min intervals for a total time of 140 min (35 frames). Two sets of experiments were performed using ^{76}Br and ^{18}F.

The axes of the phantoms were aligned with the axes of the tomographs in all the acquisitions performed. In the case of the resolution phantom, the spheres' equators were centred in the FOV.

Attenuation was measured with three external sources of germanium-68, using 60-min scans performed 12 h after emission acquisitions.

Image reconstruction. For both scanners, data were reconstructed using the protocols employed in clinical routine at our institution. The data acquired on the ECAT 953B were reconstructed using the FBP algorithm and a Hanning apodisation filter with a cut-off frequency of 0.5 cycles per pixel. No scatter correction was performed. Image reconstruction of HR+ data was done using the 3D retroprojection (3DRP) algorithm with a model-based scatter correction method [20]. Branching ratio corrections were not performed. Radioisotope decay during each acquisition frame was corrected. In this way, the different half-lives of the used radioisotopes allowed assessment of a wide range of contrasts between the spheres and the cylinder.

Data analysis. The results obtained using the 3D brain phantom were evaluated by visual inspection for qualitative image assessment. Linear profiles of the measured activities were obtained and normalised to the maximum activity on each profile. These analyses allow visualisation of the effects of the cameras and radioisotopes used on image resolution and image contrast.

Analyses of the resolution phantom images were based on a reference value for the true sphere radioactivity concentration obtained using a small ROI (0.4 cm^2) placed at the centre of the largest sphere. In order to avoid bias due to scatter, this reference value was measured on the frame for which the ratio between the radioactivity concentration in the spheres and the radioactivity concentration in the background equalled 1:1. A large ROI (14 cm^2) was used to measure the radioactivity concentration present in the background. This ROI was placed on a slice distant from those representing the spheres in order to avoid the contribution of scatter. This was especially important for ECAT 953B, for which reconstruction protocols did not include scatter correction.

The radioactivity concentrations present in the resolution phantom were measured using circular ROIs placed over each of the spheres (Table 1). The choice of different ROI sizes allowed us to evaluate, for a particular sphere, how quantitative values could be matched between acquisitions using two different radioisotopes on the same camera. The variations with time obtained for each sphere and for the cylinder radioactivity concentration were modelled with the following expression:

$$M(t)=k_1 \cdot A(t) + k_2 \cdot B(t), \quad (1)$$

where $A(t)$ represents the reference sphere activity at time t after the beginning of the dynamic study and $B(t)$ is the activity value measured for the background at the same time. $M(t)$ is the measured radioactivity concentration in an ROI for each sphere at time t and k_1 and k_2 are factors representing the contribution of the sphere activity and the influence of the background activity on $M(t)$, respectively. The k_1 coefficient, known as the hot spot recovery coefficient, represents the contrast recovery coefficient, which is independent of the background activity in the case of scatter-corrected images. The coefficient k_2, known as the cold spot recovery coefficient, represents a measure of the effect of the spill-over from background activity on the measurement of a sphere's radioactivity concentration [21, 22]. When the images are not corrected for scatter, these coefficients account not only for the quantitation biases induced by the limited resolution, but also for those induced by scatter. For each sphere and for each ROI used, k_1 and k_2 values were obtained from Eq. 1 by least squares fitting.

Table 2. Transaxial spatial resolution values for ^{76}Br and ^{18}F measured on the ECAT 953B and the HR+

	^{76}Br		^{18}F	
	Tangential	Radial	Tangential	Radial
ECAT 953B	10.7	10.3	9.2	9.0
HR+	8.2	7.8	6.8	6.5

A comparison index (CI) was defined according to the following expression:

$$CI = k_1(^{76}Br)/k_1(^{18}F), \quad (2)$$

where $k_1(^{76}Br)$ are the k_1 values obtained for ^{76}Br and $k_1(^{18}F)$ are the k_1 values obtained for ^{18}F on the same scanner. This index allows comparison of the quantitative output of ^{76}Br and ^{18}F examinations when the same structure is studied using the same tomograph and the same ROI.

Results

Measurements of spatial resolutions

The spatial resolution values were obtained by fitting gaussian functions to linear profiles drawn on a central reconstructed image slice (Table 2).

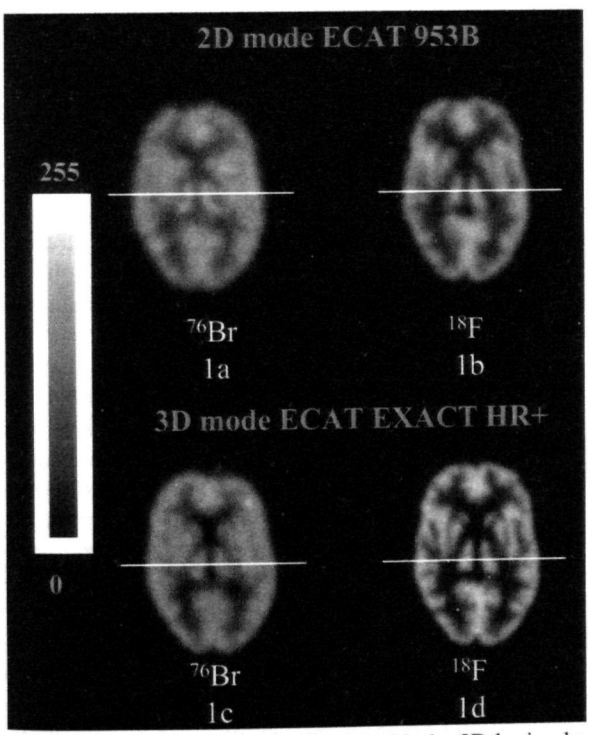

Fig. 1a–d. Transaxial slices obtained with the 3D brain phantom: **a** ^{76}Br on the ECAT 953B PET system; **b** ^{18}F on the ECAT 953B PET system; **c** ^{76}Br on the HR+ PET system; **d** ^{18}F on the HR+ PET system

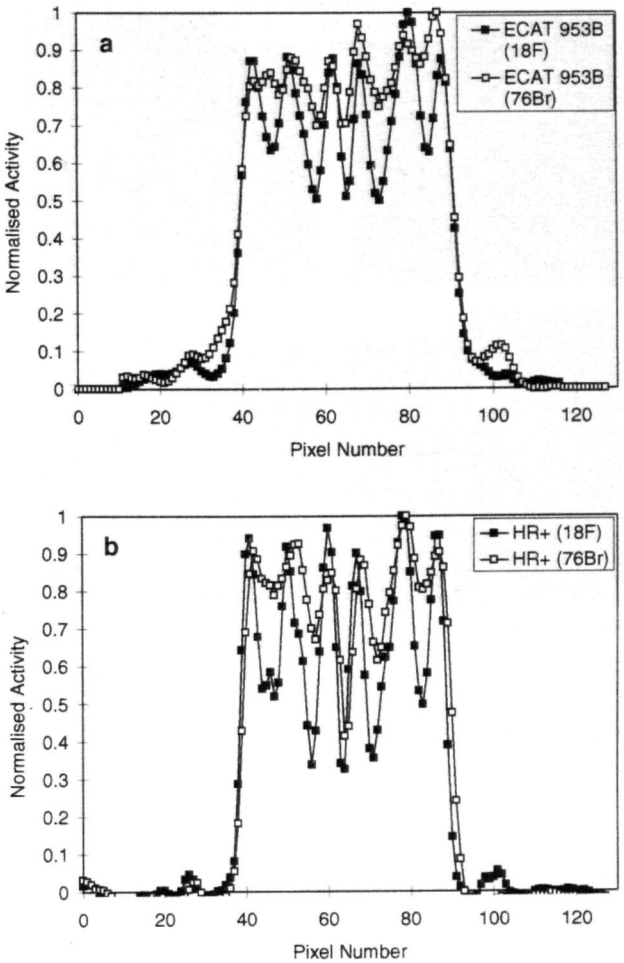

Fig. 2a, b. Linear activity profiles normalised to the maximum radioactivity present on each profile: **a** Linear activity profiles drawn on ^{18}F and ^{76}Br images obtained on the ECAT 953B PET system; **b** linear activity profiles drawn on ^{18}F and ^{76}Br images obtained on the HR+ PET system

3D brain phantom

The results obtained using the Hoffman brain phantom are shown in Fig. 1. Anatomical details were better delineated on ^{18}F images for both scanners (Figs. 1b and d). Using this radioisotope, the difference in the spatial resolution of ECAT 953B and HR+ was clearly visible. The use of ^{76}Br introduced additional blurring, leading to a significant loss of image detail in comparison with ^{18}F (Fig. 1a vs 1b and Fig. 1c vs 1d).

The dependence of image resolution and contrast on the radioisotope and scanner used can also be assessed using the profiles shown in Fig. 2. Figure 2a shows linear profiles of activity obtained from images shown in Figs. 1a and b, while Fig. 2b shows similar profiles obtained from images shown in Figs. 1c and d. The use of ^{76}Br clearly resulted in lower spatial resolution and lower image contrast than the use of ^{18}F, and this effect was visible for both tomographs used.

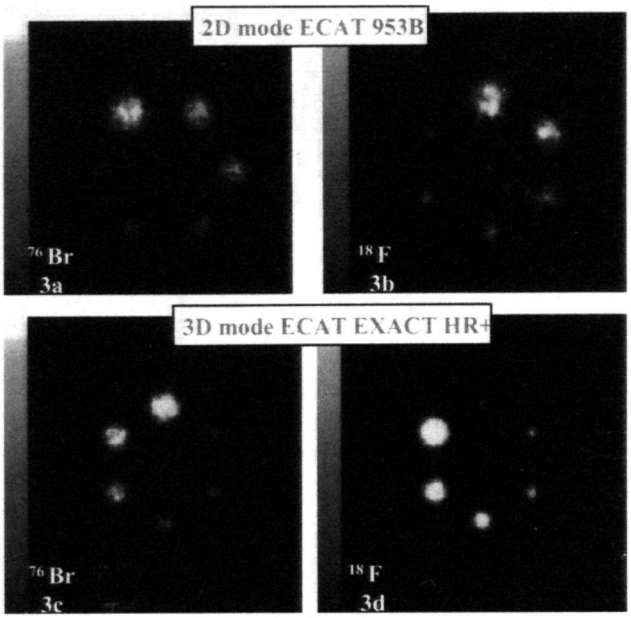

Fig. 3a–d. Transaxial slices obtained with the resolution phantom: **a** ^{76}Br on the ECAT 953B PET system; **b** ^{18}F on the ECAT 953B PET system; **c** ^{76}Br on the HR+ PET system; **d** ^{18}F on the HR+ PET system. All images were obtained for the same ratio between spheres and cylinder

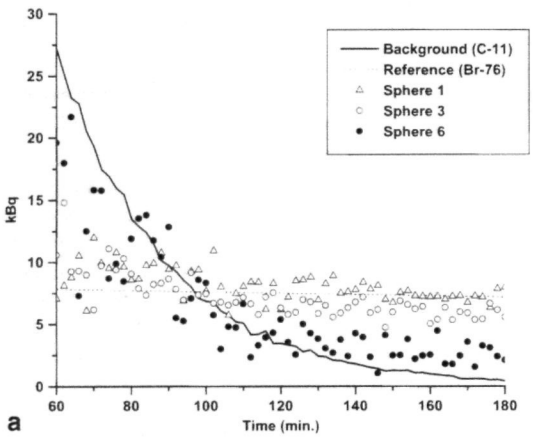

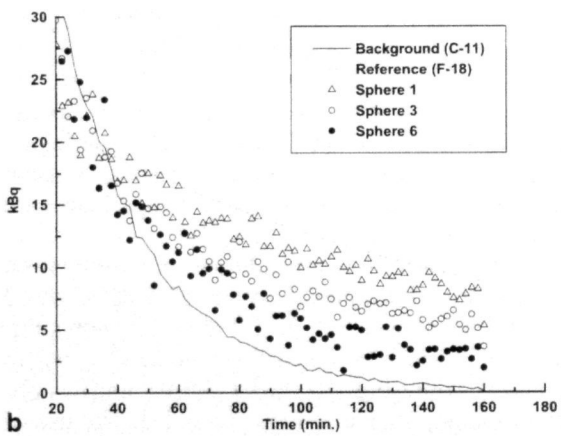

Fig. 4a, b. Variation of the radioactive concentrations in the resolution phantom measured using the ECAT 953B: **a** for ^{76}Br and ^{11}C; **b** for ^{18}F and ^{11}C

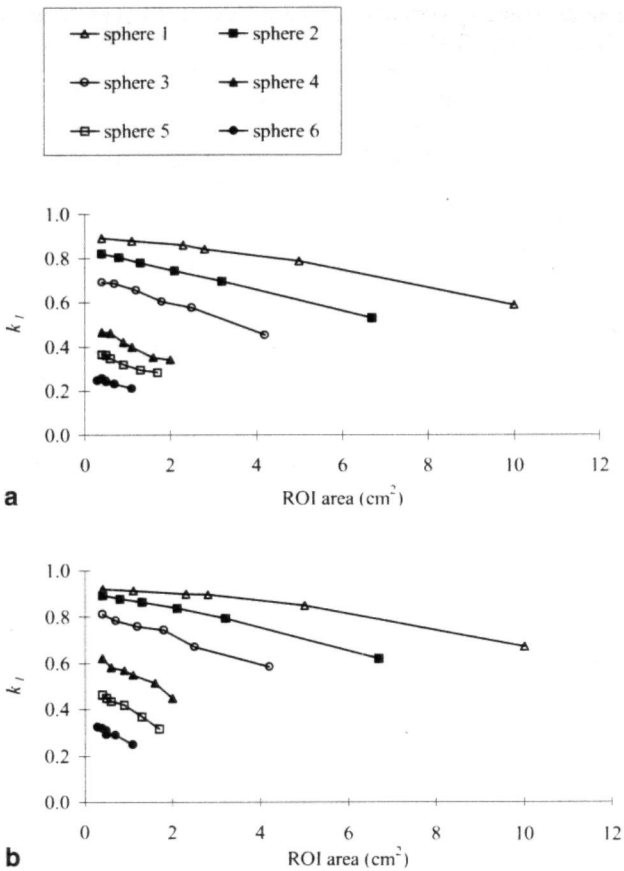

Fig. 5. k_1 values obtained for the ECAT 953B PET system using ^{76}Br (**a**) and ^{18}F (**b**)

Resolution phantom

Figure 3 shows, for the same contrast, images of the spheres obtained with ^{76}Br on the ECAT 953B (Fig. 3a) and the HR+ (Fig. 3c) and for ^{18}F on the same scanners (Fig. 3b on ECAT and Fig. 3d on HR+). Figures 4a and 4b show the variation in the radioactive concentration values measured in spheres 1, 3 and 6 (the other spheres are not represented in order to maintain graph readability) using the ECAT 953B after filling the spheres with ^{76}Br and ^{18}F respectively. An ROI of 0.4 cm^2 was used in these measurements. The corresponding reference values obtained for ^{76}Br and ^{18}F are also shown, as well as the measured variations in background activity. The curve obtained for the larger sphere shows an evolution with time which is close to that calculated for the reference activity. However, as the sphere size is reduced, the variation in the curves obtained becomes closer to that observed for the activity present on the background. These observations confirm the enhanced effects of surrounding radioactivity on the assessment of radioactivity concentration present in small structures.

Figures 5a and 5b show the evolution of k_1 values obtained for ECAT 953B using ^{76}Br and ^{18}F respectively. On Figs. 6a and 6b the corresponding variations are shown for HR+. For both tomographs, the use of ^{18}F re-

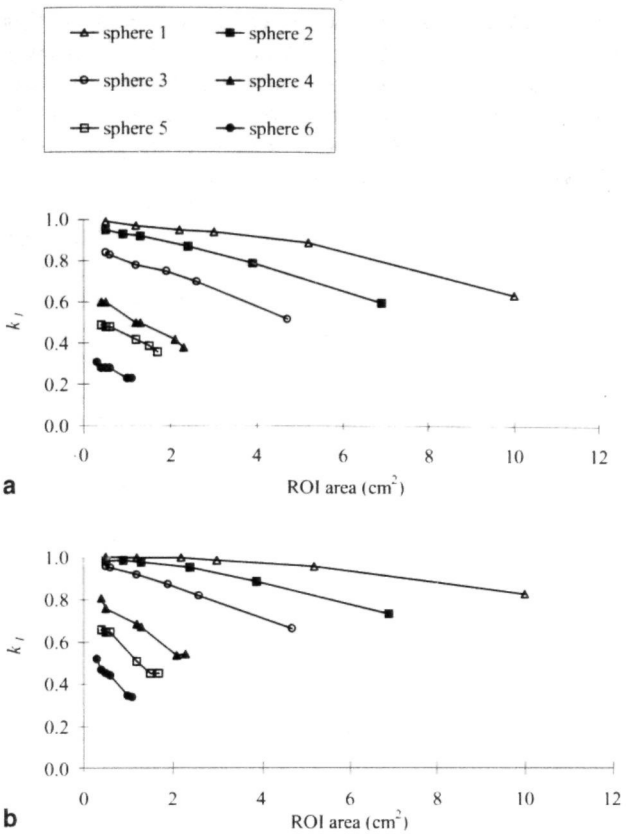

Fig. 6. k_1 values obtained for the HR+ PET system using ^{76}Br (**a**) and ^{18}F (**b**)

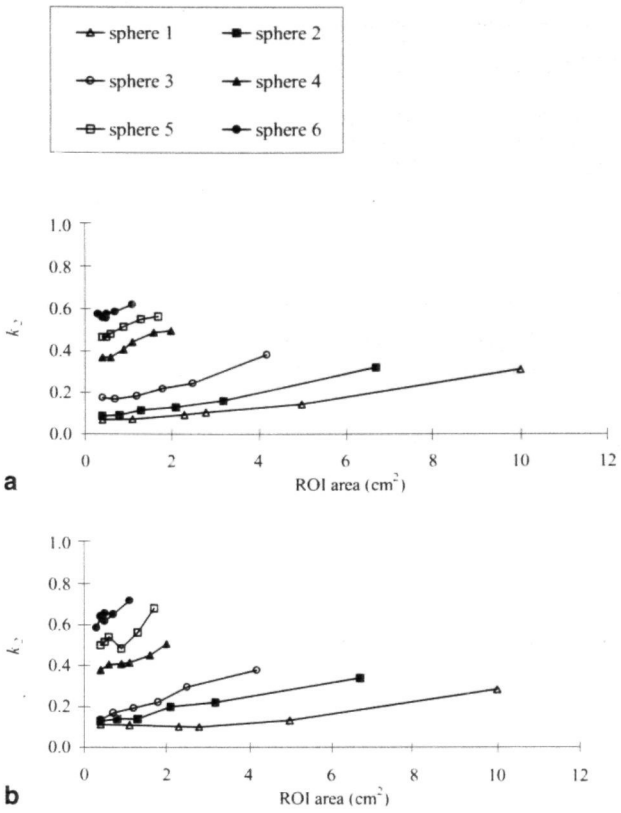

Fig. 8a, b. k_2 values obtained for the ECAT 953B PET system using ^{76}Br (**a**) and ^{18}F (**b**)

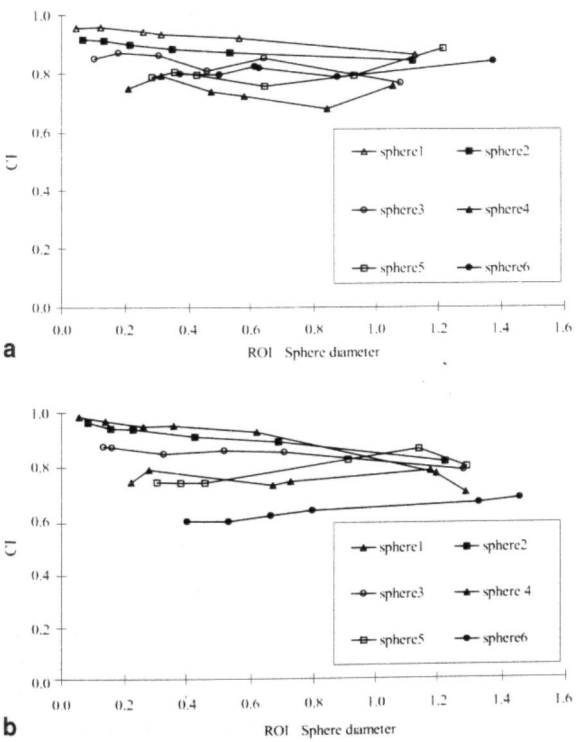

Fig. 7a, b. CI values (Eq. 2) obtained for the ECAT 953B (**a**) and the HR+ (**b**) PET systems as a function of the ratio between ROI and sphere diameter

sulted in k_1 values superior to those obtained for ^{76}Br. In the case of ECAT 953B and for the larger spheres, this difference was small for almost all ROI tested. Differences between the use of the two radioisotopes became evident for the smaller spheres when the same ROI was used. These differences were increased by reduction in ROI size and may be attributed to resolution losses resulting from the different range in matter of the positrons emitted by each radioisotope. The dependence of k_1 values on ROI size was more significant when using ^{18}F, resulting in more marked curve slopes. The variation of k_1 obtained for HR+ (Fig. 6) showed essentially the same trend as that described for ECAT 953B but values were higher for smaller spheres and systematically closer to 1 for larger spheres. The use of HR+ resulted in more marked differences between the k_1 values obtained using ^{76}Br and ^{18}F on smaller spheres.

Values of CI calculated using Eq. 2 are shown in Fig. 7 as a function of the ratio between ROI diameter and sphere diameter. As expected, the CI values were generally higher for ECAT953 (Fig. 7a) than for HR+ (Fig. 7b) when imaging the smaller spheres.

Figures 8a and 8b show the evolution of k_2 values for each sphere as a function of the ROI size for ECAT 953B and when using ^{76}Br and ^{18}F respectively. On Figs. 9a and 9b the corresponding variations are shown for HR+. For ECAT 953B, small differences were ob-

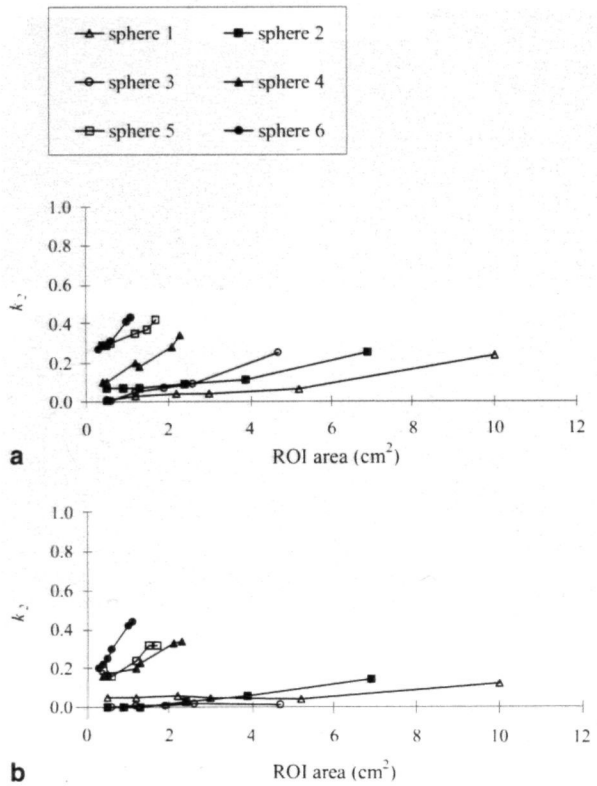

Fig. 9a, b. k_2 values obtained for the HR+ PET system using ^{76}Br (**a**) and ^{18}F (**b**)

served between ^{76}Br and ^{18}F. The k_2 values measured for HR+ were lower than those measured for ECAT 953B for both radioisotopes present inside the spheres.

Discussion

The main objective of this study was to compare the use of ^{76}Br and ^{18}F for the quantification of small structures in PET. We chose to perform the study using reconstruction protocols currently applied in clinical routine. The use of two different PET machines with different intrinsic spatial resolution showed how the different physical characteristics of the two radioisotopes chosen could influence the quantitative output obtained for the same structure analysed using the same ROIs.

The images of the 3D brain phantom showed that the use of ^{76}Br and ^{18}F on the same scanner yields varying results. Despite the use of the same reconstruction conditions, the images obtained using ^{76}Br showed greater blurring than those obtained using ^{18}F. The linear profiles of activity calculated for each tomograph/radioisotope combination confirmed the visual assessment and indicated that the use of ^{76}Br introduces additional contrast and spatial resolution degradation as compared with ^{18}F.

Using a phantom simulating small structures in a background of variable activity, we studied the influence of two different positron ranges on the values of the hot spot recovery coefficient k_1. This evaluation was done in parallel on two different scanners. Since we were not comparing machine performance, we needed only to ensure that identical ROIs were used for the analysis of ^{76}Br and ^{18}F acquisitions performed on the same machine. We used ROIs of the same size to study structures of the same dimensions, (i.e. the same sphere) imaged using different radioisotopes on the same machine. Since the spheres were located at the same radial position, the radial variation of the on spatial resolution affected similarly all the structures studied. As expected, the measured k_1 values increased with object size for the same ROI. The k_1 values obtained with ^{18}F led to systematically higher values than where measured with ^{76}Br even if ROIs of similar size were used for image analysis. This observation was valid for both scanners and may have important consequences when quantitation values obtained from acquisitions using the same scanner but different radioisotopes are to be compared. The differences between the results obtained using ^{76}Br and ^{18}F were more significant for data acquired on the scanner with better spatial resolution (HR+).

Since ^{76}Br and ^{18}F images were obtained using the same reconstruction parameters on each scanner, the differences observed in quantitative accuracy when using the same ROI may have resulted from the different positron ranges characteristic of each radioisotope. Longer positron ranges average the object activity over larger volumes. Therefore, even if the system response function has the same shape (that is, even if the same camera is used), its FWHM is artificially enlarged when using higher energy positron emitters. This effect was verified during the spatial resolution measurements performed on both scanners. These results showed that the quantitation of an object depends on the radioisotope used, especially for small structures. This observation led us to investigate how the ROI size could be used to match the quantitative results obtained for a particular structure imaged with different radioisotopes. The calculation of CI (Eq. 2) allowed assessment of the differences in k_1 values obtained using ^{76}Br and ^{18}F as a function of the ratio between the ROI diameter and the sphere diameter. This index could be used as a correcting factor in order to "normalise" ^{76}Br and ^{18}F studies of the same structures which had been analysed using the same ROI.

The k_2 values reflect the influence of background radioactivity on the radioactivity concentration measured in each sphere. The calculation of k_2 values depends dramatically on the first time frames of each acquisition. In fact, it is for these time frames that the background activity is higher and therefore generates significant spillover. Since the total activity present at these early times is important, the large amount of random coincidences detected is likely to give rise to the fluctuations that we observed for k_2. For the same radioisotope, k_2 values were higher for studies performed on the ECAT 953B, which can be attributed to the worse resolution of this

tomograph. For the same tomograph, k_2 values were similar for the two radioisotopes, which reflects the fact that the same radionuclide (^{11}C) was used for background activity. Since the positron range of ^{11}C is similar to that of ^{18}F, there should be no significant differences if ^{18}F is used as background activity. However, since ^{76}Br has a longer positron range than ^{11}C, one would expect an increase in the k_2 values of a given tomograph if ^{76}Br is used as background activity, especially for the smaller spheres.

Reconstructions used the same parameters as the clinical protocols. Since scatter correction was used on the HR+ (3D acquisition mode), we assumed that the parameters calculated on this scanner were free from the influence of scatter. Scatter was present on the acquisitions performed on the ECAT 953B. However, the use of the 2D mode significantly reduces the detection of scattered events. Furthermore, the spheres were located at the same radial position allowing us to assume that the scatter distribution was approximately axially symmetrical. Moreover, since the reference value for the true activity was obtained from an ROI placed in the largest sphere and without the use of scatter correction, we estimate that the presence of scatter would not have had a significant impact on coefficient values obtained for ECAT 953B.

In earlier studies, the practical impact of positron range on the resolution of PET scanners was considered of minor significance. This was essentially due to the relatively low intrinsic system resolutions available at that time (8–12 mm). However, the recent generation of PET scanners has reached intrinsic resolutions of between 2 mm (animal PET scanners) and 5 mm, and the effects of positron range on image quality must therefore be re-evaluated.

The results obtained in this study show that the positron range has a significant impact on the quantitative values obtained in PET and that this effect becomes more important with increased intrinsic camera resolution, especially for smaller structures. If a precise comparative analysis of images obtained using different radioisotopes is to be performed, adaptation of ROI size or the use of a correction factor which takes into account the differences in positron range between the radioisotopes used in each study may be mandatory.

Acknowledgements. We are greatly indebted to the chemical and cyclotron staff of Service Hospitalier Frédéric Joliot, Orsay, France. M.-J.R., P.A. and N.F. were partially supported by Fundação para a Ciência e Tecnologia (Portugal) (PhD grants #PRAXIS-XXI/BD/2657/94, #PRAXIS-XXI/BD/3300/94 and #PRAXIS-XXI/BD/2656/94, respectively). M.-J.R. and N.F. were also supported by A.R.S. (Portugal).

References

1. Price P. Is there a future for PET in oncology? *Eur J Nucl Med* 1997; 24: 587–589.
2. Garnett ES, Firnau G, Nahmias C. Dopamine vizualized in the basal ganglia of living man. *Nature* 1983; 305: 137–138.
3. Brooks DJ, Ibanez V, Sawle GV, Quinn N, lees AJ, Mathias CJ, Bannister R, Marsden CD, Frackowiak RSJ. Differing patterns of striatal ^{18}F-DOPA uptake in Parkinson's disease, multiple system atrophy and progressive supranuclear palsy. *Ann Neurol* 1990; 28: 547–555.
4. Mazière B, Loc'h C, Hantraye P, Guillon R, Duquesnoy N, Soussaline F, Naquet R, Comar D, Mazière M. ^{76}Br-bromospiroperidol: a new tool for quantitative in vivo imaging of neuroleptic receptors. *Life Sci* 1984; 35: 1349–1356.
5. Loc'h C, Mardon K, Valette H, Brutesco C, Merlet P, Syrota A, Mazière B. Preparation and pharmacological characterization of [^{76}Br]-meta-bromobenzylguanidine ([^{76}Br]MBBG). *Nucl Med Biol* 1994; 21: 49–55.
6. Kassiou M, Loc'h C, Strijckmans V, Katsifis A, Lambrecht RM, Mazière M, Mazière B. Synthesis of [^{76}Br]4-bromodexetimide and [^{76}Br]4-bromolevetimide: radiotracers for studying muscarinic cholinergic receptors using PET. *J Lab Comp Radiopharm* 1995; XXXVI: 259–266.
7. Mazière B, Loc'h C, Bourguignon M, Raynaud C, Hantraye P, Martinot JL, Syrota A, Mazière M. PET and SPECT imaging of D_2 brain receptors in baboon and human brain using ^{76}Br- and ^{123}I-lisuride. *Eur J Nucl Med* 1989; 15: 403.
8. Loc'h C, Halldin C, Bottlaender M, Swahn CG, Moresco RM, Mazière M, Farde L, Mazière B. Preparation of ^{76}Br-FLB 457 and ^{76}Br-FLB 463 for examination of striatal and extrastriatal dopamine D_2 receptors with PET. *Nucl Med Biol* 1996; 23: 813–819.
9. Kuwert T, Sures T, Herzog H, Loken M, Hennerici M, Langen KJ, Feinendegen LE. On the influence of spatial resolution and the size and form of regions of interest on the measurement of regional cerebral metabolic rates by positron emission tomography. *J Neural Transm* 1992; 37: 53–66.
10. Weckesser M, Hufnagel A, Ziemons K, Griesmeier M, Sonnenberg F, Hacklander T, Langen KJ, Holschbach M, Elger CE, Muller-Gartner HW. Effect of partial volume correction on muscarinic cholinergic receptor imaging with single-photon emission tomography in patients with temporal lobe epilepsy. *Eur J Nucl Med* 1997; 24: 1156–1161.
11. Haber SF, Derenzo SE, Uber D. Application of mathematical removal of positron range blurring in positron emission tomography. *IEEE Trans Nucl Sci* 1990; 37: 1293–1299.
12. Levin CS, Hoffman EJ. Calculation of positron range and its effect on the fundamental limit of positron emission tomography system spatial resolution. *Phys Med Biol* 1999; 44: 781–799.
13. Pagani M, Stone-Elander S, Larsson SA. Alternative positron emission tomography with non-conventional positron emitters: effects of their physical properties on image quality and potential applications. *Eur J Nucl Med* 1997; 24: 1301–1327.
14. Spinks TJ, Jones T, Bailey DL, Townsend DW, Grootoonk S, Bloomfield PM, Gilardi MC, Casey ME, Sipe B, Reed J. Physical performance of a positron tomograph for brain imaging with retractable septa. *Phys Med Biol* 1992; 37: 1637–1655.
15. Mazoyer B, Trébossen R, Deutch R, Casey M, Blohm K. Physical characteristics of the ECAT 953B/31: a new high resolution brain positron tomograph. *IEEE Trans Med Imaging* 1991; 10: 499–504.

16. Bendriem B, Trébossen R, Frouin V, Lamer O, Brulon V, Syrota A. Evaluation of a PET scanner in 2D and 3D acquisition mode. *Proc IEEE Eng Med Biol Soc* 1992; 5: 1837–1840.
17. Adam LE, Zaers J, Ostertag H, Trojan H, Bellemann ME, Brix G. Performance evaluation of the whole-body PET scanner ECAT EXACT HR+ following the IEC standard. *IEEE Trans Nucl Sci* 1997; 44: 1172–1179.
18. Brix G, Zaers J, Adam LE, Bellemann ME, Ostertag H, Trojan H, Haberkorn U, Doll J, Oberdorfer F, Lorenz WJ. Performance evaluation of a whole-body PET scanner using the NEMA protocol. *J Nucl Med* 1997; 38: 1614–1623.
19. Hoffman EJ, Cutler PD, Digby WM, Mazziotta JC. 3-D phantom to simulate cerebral blood flow and metabolic images for PET. *IEEE Trans Nucl Sci* 1990; 37: 616–620.
20. Watson CC, Newport D, Casey ME. A single scatter simulation technique for scatter correction in 3D PET. 1995 international meeting on fully three-dimensional image reconstruction in radiology and nuclear medicine 1995, Aix-les-Bains, Savoie, France: 215–219.
21. Kessler RM, Ellis J, Eden M. Analysis of emission tomographic scan data: limitations imposed by resolution and background. *J Comput Assist Tomogr* 1984; 8: 514–522.
22. Links JM, Zubieta JK, Meltzer CC, Stumpf MJ, Frost JJ. Influence of spatially heterogeneous background activity on "hot object" quantitation in brain emission computed tomography. *J Comput Assist Tomogr* 1996; 20: 680–687